Renewable and Sustainable Energy Transition 3 (2023) 100053

Contents lists available at ScienceDirect

Renewable and Sustainable Energy Transition

journal homepage: www.journals.elsevier.com/renewable-and-sustainable-energy-transition

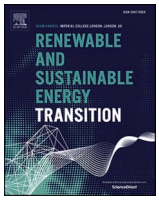

Full-length article

Planning third generation minigrids: Multi-objective optimization and brownfield investment approaches in modelling village-scale on-grid and off-grid energy systems

Nicolò Stevanato [a,*], Gianluca Pellecchia [a], Ivan Sangiorgio [a], Diana Shendrikova [a], Castro Antonio Soares [a,b], Riccardo Mereu [a], Emanuela Colombo [a]

[a] Department of Energy, Politecnico di Milano, Milan, Italy
[b] FUNAE - Fundo de Energia, Maputo, Mozambique

ARTICLE INFO

Keywords:
Microgrid
Access to energy
Rural electrification
Multi-objective optimization
Brown-field investment

ABSTRACT

Access to reliable and sustainable electricity is still precluded for a large share of global population living in rural areas of developing countries, especially in sub-Saharan Africa. Hybrid microgrids are considered a suitable solution for providing affordable and reliable access to electricity to isolated communities. Properly planning and sizing such systems is although an aspect that can greatly influence the sustainability of the intervention, and the arrival to the market of the third generation minigrids poses new challenges to the process. Three main challenges are identified as pivotal for the proper sizing of new generation microgrids: arrival of the main grid, inappropriateness of Net Present Cost as only objective function in the strategy selection process, and necessity to operate on already existing minigrids. Such aspects are addressed in this work by proposing a methodological advancement to an existing open-source microgrid sizing model: a grid outage model alongside the definition of new constraints and variables for the optimization problem with grid-connected microgrids, a multi-objective optimization option, and a brown-field optimization option. The new version of the model is tested on real life case studies in rural Rwanda (greenfield) and Mozambique (brownfield), proving the profitability of grid-connected and grid-extension solutions for sufficiently low connection distances. Sensitivity analyses are performed to assess variations in system size, cost and CO_2 emissions with respect to microgrid and grid connection parameters.

1. Introduction

As remarked during the last COP26 in Glasgow, in the global discourse around the Energy Transition that the world will need to undergo, universal access to energy is a fundamental aspect that cannot be neglected [1]. As highlighted by the IEA and IRENA in their last joint report, still 759 million people lacked access to a reliable and sustainable source of electricity [2]. The main share, namely 75%, of this population is located in Sub Saharan Africa, and 84% of the population with no access resides in rural areas of the continent [3].

Among the existing technological solutions, microgrids proved to be particularly suitable for granting access to populations that reside in rural area, and hence distant from the national T&D grids, and that present high population density and demand [4]. According to the World Bank, microgrids are expected to represent the solution for alleviating the issue of lacking access to electricity for "half a billion people" worldwide [5].

Microgrids are stand-alone electricity supply systems, that can count from some kW up to few MW of supply capacity [4]. Originally they were mainly diesel generator based, but in the last decade microgrids are more and more deployed in hybrid forms, including solar PVs, wind turbines and pico-hydro turbines, depending on the resource availability of the area [6]. Finally, the most recent and so-called *third generation microgrids* [7] are designed to be ready for eventual connection to the national grid, representing a huge step forward considering the issue that has been in the past the arrival of the main grid to a village powered by a microgrid [8].

The design of reliable and appropriate off-grid energy system is usually critical. The energy needs of people who are susceptible to the uncertainty of possible energy consumption evolution through time

* Corresponding author.
E-mail address: nicolo.stevanato@polimi.it (N. Stevanato).

https://doi.org/10.1016/j.rset.2023.100053
Received 4 August 2022; Received in revised form 23 February 2023; Accepted 9 March 2023
Available online 14 March 2023

must be considered, taking into consideration site-specific characteristics of each target community [9].

In this field, energy system models can play a pivotal role in guiding informed policy decisions trying to capture the complexities related to the time-evolving boundary conditions, comparing alternative energy system configurations and energy mix combinations to find the optimal solution, as thoroughly reviewed in a recent publication that categorizes 111 studies that adopt optimization models for rural electrification support [10].

Four main challenges are identified by the authors in current state of the art microgrid optimal sizing tools, presented below.

(i) *Net Present Cost alone is not a sufficient decision parameter in energy system sizing*:

Most optimization tools are focused on single-objective optimization that does not allow to capture the complexity of an intervention of rural electrification. Multi-objective optimization could be a solution to address economic, social and environmental objective evaluating different trade-off between these criteria, especially in the rural electrification sector where different stakeholders (companies, public institutions, NGOs) with different priorities are involved. This is crucial in this type of projects given the multiplicity of impacts on the community involved and the interconnection between them. The result of multi-objective optimization would be a Pareto frontier providing the decision maker with a more comprehensive view of the possible alternatives and allowing him to take more informed decisions. Exceptions to this are represented by Dufo-Lopez [11] that included a multi objective optimization on NPC, HDI and Job Creation and Petrelli [12] that optimizes on NPC, LCA emissions, Land Use and Job Creation.

(i) *Third generation minigrids and the arrival of the main grid*:

It has been observed how the arrival of the main grid at the microgrid location causes issues such as technology abandonment [8]. But the arrival of the main grid can be an asset, third generation microgrids are built with a compatibility with the connection to the national grid [7] and sizing a microgrid from the first year considering that at a given year the national grid will arrive is a key aspect that can grant a strategic advantage to the planning of the system. Exception is made for Homer® PRO [13], a diffuse proprietary software developed by NREL.

(i) *The necessity to operate on already existing minigrids*:

From the review of the literature [10] regarding the energy system optimization models, it is noticed the absence of tools to design and optimize a so-called Brownfield Investment. Brownfield investment is the act of purchasing or leasing existing production facilities to launch a new production activity, this is a strategy used in foreign direct investment [14]. The alternative to this is a greenfield investment, in which a new plant is constructed. The clear advantage of a brownfield investment strategy is that the facilities are already constructed. The costs and time of starting up may thus be greatly reduced and the plant already up to code. Only Alsaidan [15] proposes a storage system expansion optimization.

Finally, Jaszczur [16] proposes a NPC—CO_2 optimization also for grid-connected systems but only optimizes the sizing, without the dispatch, grid reliability is not modelled, and brownfield is not an optimization option.

Building on previous modelling experience of the authors [17–19] the proposed methodology is implemented into the modelling framework MicrogridsPy [20]. It is an open-source python-based model conceived for the optimization of hybrid electric microgrids, including solar PV, wind turbines, diesel genset and batteries.

MicroGridsPy model provides a solution to the problem of sizing and dispatch of energy in microgrids in isolated places at village scale with a time resolution of 1 hour and time evolving load demand. The model is based on two-stage stochastic optimization, where the main optimization variables are divided into first-stage variables (rated capacities of each energy source) and second-stage variables (energy flows from the different components), to deal with the high level of uncertainty associated with renewable energy potential forecasts and the complex dynamics that govern the current and future evolution of electricity consumption in rural settings (parametric uncertainty) [21], while LP or MILP formulation can be used to tackle the imperfect mathematical representation of component operation (structural uncertainty), mainly related to the modelling of non-linear behavior. The optimization is performed in Python using Pyomo Library. Energy balance, VRES generation constraints, Battery charge/discharge constraints, Genset generation constraints are the main constraints of the model while regarding the objective function, it's possible to switch between NPC and Operation Cost minimization.

The work presented will add to existing knowledge in the following ways:

(i) It will introduce a multi-objective optimization option to the tool, adding CO_2 emissions of generation technologies to the already existing NPC objective function.
(ii) It will include in the tool the possibility to account for the arrival of the main grid to the microgrid at a given year, accounting for the possibility to purchase from the grid and sell to the grid at different prices, and to model the national grid reliability.
(iii) It will include the possibility to optimize a brownfield intervention to an existing microgrid, namely taking into account already installed generation and storage capacity of the system.

The remainder of the paper is structured as follows: Section 2 will describe the methodology adopted to implement the features in the model, Section 3 presents the two case studies to which the model is applied to and Section 4 reports the respective results. Finally, Section 5 draws conclusions and policy implications deriving from the study.

2. Methodology

2.1. Multi objective

A generic multi-objective optimization can be expressed as follows (considering minimization problem):

$$\begin{aligned} &\min f(\boldsymbol{x}) = \left[f_1(\boldsymbol{x}), f_2(\boldsymbol{x}), \ \ldots, f_j(\boldsymbol{x})\right] \\ &s.t. \ \ y_i\ (\boldsymbol{x}) \leq 0 \ i \in 1 \ldots m \\ &h_l\ (\boldsymbol{x}) = 0 \ l \in 1 \ldots q \\ &\boldsymbol{x} = [x_1, x_2, \ldots, \ x_n] \end{aligned} \tag{1}$$

where $f(\boldsymbol{x})$ is the j-dimensional vector of the objective functions, dependent on the n-dimensional vector of decision variables $\boldsymbol{x}$. The problem is subject to m inequality constraints and q equality constraints. The goal of multi-objective optimization is to find the solutions as close as possible to the Pareto frontier.

The Pareto frontier is composed by the set of so-called non-dominated points, i.e. solutions in which the performance of one objective function cannot be improved without worsening at least one other objective function [22,23]. The most used and efficient algorithms for the solution of multi-objective problems are the weighted sum method [24,25], which is typically used when the objective functions belong to the same sphere of interest, and the ε-constrain method [26–28], which

is able to represent the entire pareto frontier independently from its shape and will be adopted in this study.

The ε-constrain method transforms the multi-objective optimization in several single-objective optimization. For sake of simplicity, two objective functions are considered, and process is shown in Algorithm 1.

Firstly, the optimization of the first objective function $f_1(\boldsymbol{x})$ is performed to evaluate simultaneously the minimum value of $f_1(\boldsymbol{x})$ and the maximum value of $f_2(\boldsymbol{x})$, named $\overline{f_2}$. Therefore, the optimization of $f_2(\boldsymbol{x})$ follows determining the minimum value of $f_2(\boldsymbol{x})$, named $\underline{f_2}$, and the maximum value of $f_1(\boldsymbol{x})$. At this point according to the number of possible solutions (p) on the Pareto frontier the user wants to analyze, the range between $\underline{f_2}$and $\overline{f_2}$ is divided into (p-1) intervals, with a resolution of $step = \frac{r_2}{p-1}$, where $r_2 = \left(\overline{f_2} - \underline{f_2}\right)$ represents the range of variation of $f_2(\boldsymbol{x})$, in order to obtain a p-dimensional vector F_2, which contain all the equidistant values of $f_2(\boldsymbol{x})$, included $\underline{f_2}$and $\overline{f_2}$. An iteration cycle with single-objective optimization using $f_1(\boldsymbol{x})$ as objective function can be performed taking into consideration $f_2(\boldsymbol{x})$ as equality constraint, changing at each iteration it its value, as shown in Eq. (2). For every iteration it, the values of $f_2(\boldsymbol{x})$ is updated and equal to $F_2(it)$, where $it \in \{1,\ldots,p\}$.

$$
\begin{aligned}
&\min f_1(\boldsymbol{x}) \\
&s.t.\ \ f_2(\boldsymbol{x}) = F_2(it)\ \ it \in 1\ldots p \\
&y_i\ (\boldsymbol{x}) \le 0\ \ i \in 1\ldots m \\
&h_l\ (\boldsymbol{x}) = 0\ \ \in 1\ldots q \\
&\boldsymbol{x} = [x_1, x_2, \ldots .,\ x_n]
\end{aligned}
\tag{2}
$$

In this work the two objective functions taken into consideration are the Net Present Cost (or the Operation Cost) and the CO_2 emissions to focus simultaneously on economic and environmental aspects, with the latter that has gained a greater interest in the last years. In particular, Life Cycle Assessment could be taken into account to quantify the emissions along the whole life-cycle of the assets and not only the direct emissions from the operation of the energy systems in order to avoid incomplete and misleading evaluations. In case single-objective optimization (minimization of NPC) is selected, the CO_2 emissions of the optimal configuration are computed according to the capacity installed of each component and to the optimized operational dispatch strategy.

To perform an accurate evaluation of the microgrid impact, emissions have been considered in terms of LCA, i.e. accounting for construction, installation, operation and disposal of the assets. CO_2 emissions related to the transportation of fuel and technologies are not considered because too specific to the location and difficult to assess accurately. The mathematical formulation of CO_2 emissions for each component c is reported in Eqs. (3)–(5), where e^c is the specific emissions of each component.

Algorithm 1
ε-constrain method with two objective functions.

1: *Calculate bounds:* $\underline{f_1} = \min f_1(\boldsymbol{x})$ *and* $\overline{f_2} = \max f_2(\boldsymbol{x})$ *with* $f_1(\boldsymbol{x})$ *as objective function*
2: *Calculate bounds:* $\underline{f_2} = \min f_2(\boldsymbol{x})$ *and* $\overline{f_1} = \max f_1(\boldsymbol{x})$ *with* $f_2(\boldsymbol{x})$ *as objective function*
3: *Initialize* F_1 *and* F_2
4: *Ask to the user how many solutions (p) on the Pareto Frontier would analyze*
5: *Calculate step* $= \dfrac{r_2}{p-1}$ *to create* F_2
6: ***for*** $it \in \{1,\ldots,p\}$
7: *Solve* (2) *to obtain* $F_1(it)$ *with* $f_2(\boldsymbol{x}) = F_2(it)$
8: *add* $F_1(it)$ *to* F_1
9: ***End***
10: *Display* F_1 *and* F_2 *and plot the Pareto Frontier*
11: *Ask which couple of values satisfy the requests of the user*
12: *Print out the results*

$$
\begin{aligned}
CO2^{res} = &\sum_{r}^{R}\left(e_r^{res}\cdot\left(N_{r,u=1}^{res} - N_r^{res,inst}\right)\cdot C_r^{res,unit}\right) \\
&+ \sum_{r}^{R}\left(e_r^{res}\cdot\sum_{u=2}^{steps}\left(N_{r,u}^{res} - N_{r,u-1}^{res}\right)\cdot C_r^{res,unit}\right)
\end{aligned}
\tag{3}
$$

$$
CO2^{batt} = e^{batt}\cdot\left(C_{u=1}^{batt,nom} - C^{batt,nom}\right) + \sum_{u=2}^{steps}\left(C_u^{batt,nom} - C_{u-1}^{batt,inst}\right)
\tag{4}
$$

$$
\begin{aligned}
CO2^{gen} = &\sum_{g}^{G}\left(e_g^{gen}\cdot\left(C_{g,u=1}^{gen,nom} - C_{g,u}^{gen,inst}\right)\right) \\
&+ \sum_{g}^{G}\left(e_g^{gen}\cdot\sum_{u=2}^{steps}\left(C_{g,u}^{gen,nom} - C_{g,u-1}^{gen,nom}\right)\right)
\end{aligned}
\tag{5}
$$

Where $CO2^{res}$, $CO2^{batt}$ and $CO2^{gen}$ are, respectively, the CO_2 emissions related to the installation of, respectively, the renewable components, the batteries and the generators. Furthermore, e_r^{res}, e^{batt} and e_g^{gen} expressed in $\left[\frac{ton_{CO_2}}{kW}\right]$ are the specific emissions related with the installation of the component. The three equations are structured in the same way, and Eq. (3) can be used to explain the logic. The emissions related with the installation of all the renewable components R is the sum of the emissions related with the installation of all the r components. The emissions related to every r component are calculated as the sum of two different installation periods: i) the first round of installation when the first batch of units $N_{r,u=1}^{res}$ installed during investment period $u = 1$ reduced by the already existing units $N_r^{res,inst}$ in case of brownfield and ii) the marginal increase of unit of every following investment period $\sum_{u=2}^{steps}(N_{r,u}^{res} - N_{r,u-1}^{res})$ both multiplied by the size of the unit in $[kW]$.

The fuel-fired generators and the electricity supplied by the national grid are the only contributing emissions during the operational phase and are calculated in Eqs. (6) and (7).

$$
CO2_s^{fuel} = \sum_{g}^{G} e_g^{fuel}\cdot\left(\sum_{y}^{years}\left(\sum_{t}^{periods}\frac{E_{s,g,y,t}^{gen}}{\eta_g^{gen}\cdot LHV_g^{fuel}}\right)\right)
\tag{6}
$$

$$
CO2_s^{grid} = e^{grid}\cdot\left(\sum_{y}^{years}\left(\sum_{t}^{periods}E_{s,y,t}^{fromGrid}\right)\right)
\tag{7}
$$

In each investment decision phase, CO_2 emissions are calculated based on the capacities installed. The capacity previously installed for each technology is not considered in the computation of CO_2 emissions linked to the manufacture, installation and operation of each technology when brownfield investment optimization is used. The model also gives the possibility to consider only direct emissions due to fuel-fired generators (diesel specific emissions equals to 3.15 $kgCO_2$/lt) and to the electricity purchased from the grid (specific emissions in Section 2.1.1), neglecting the LCA emissions connected to the construction, installation and disposal of the technologies.

The extreme solutions *Min_NPC* and Min_CO_2 on the curve represent the single-objective optimization results referred, respectively, to the minimization of NPC and CO_2 emission. Both optimal Pareto frontiers have an exponential trend because in order to reduce CO_2 emissions, a slight increase in the NPC is required in the first instances, while after the first points, a significant increase in the NPC, mainly due to deployment of progressively larger capacity of cost-ineffective technologies like WT, is required for further emission reduction thanks to its low specific emission. This is evident looking to the differential increment/decrement of emission and NPC passing from the point at minimum NPC to the one at minimum emissions on the curve with LCA emissions used as example. From SIN*GLE_NPC* to *MULTI_1* the CO_2 emissions decrease of 224.44 ton while the NPC increases of 1.7%. On the other side, from *MULTI_3* to SIN*GLE_CO2*, with the same decrease of emission, the NPC increases of 47.1%. This trend can be observed between all the

consecutive points and it is emphasized when the multi-objective optimization is applied to the brownfield investment case, as can be seen in some of the following case studies. Consequently, it's evident that the point at minimum CO_2 has important drawbacks related to the resulting large NPC. The same trend can be noticed in the case with direct emissions only.

2.1.1. National grid emissions

In order to include in the analysis the direct CO_2 emissions of the electricity supplied by the national grid, direct emissions related to national electricity generation are computed. Given the geographical scope of this study, the direct emissions of the national power systems of the 54 African Countries are computed. Indeed, the open-source nature of the tool allows future users to include emissions of different countries if needed.

To calculate the direct emissions of the country's power systems each country electricity mix is derived from the IEA Data & Statistics tool [29], and for the countries not available, from the IRENA country profiles [30]. Retrieved the electricity mix of the 54 countries, the assumptions contained in Tables 1 and 2 are used to estimate the carbon intensity of the electricity sector.

In Table 1 CH*P* stands for *Combined Heat and Power* and *CCGT* to *Combined Cycle Gas Turbine* as defined by the International Energy Agency Energy Technology Systems Analysis Program [31,32].

The full list of countries with relative electricity generation and calculated CO_2 emissions is reported in Supplementary File SF-1. The calculated country-specific direct CO_2 emissions e^{grid} are used in Eq. (7) to compute the total direct CO_2 emitted by the microgrid due to the usage of national grid energy.

2.2. On-grid

The reliability of national grid electricity supply has been accounted considering a 8760 h $\times$ $T_{project}$ matrix **G** (being $T_{project}$ the microgrid lifetime in years) filled with boolean values and representing the availability of the grid in a given hour of the year. The procedure applied for the calculation of **G** is based on grid power outages modelling by [21], in which the variables Outage Duration (OD) and Time Between Outages (TBO) are assumed to follow a two-parameters Weibull probability distribution. The use of Weibull distribution is consolidated in literature to model the behavior of components failure [35]. Weibull probability density function for a random variable X, defined for $t \geq 0$, is given by:

$$f(t) = \frac{k}{\lambda}\left(\frac{t}{\lambda}\right)^{k-1} exp\left(-\left(\frac{t}{\lambda}\right)^{k}\right) \tag{8}$$

and its cumulative distribution function (CDF) is:

$$f(t) = 1 - exp\left(-\left(\frac{t}{\lambda}\right)^{k}\right) \tag{9}$$

where λ and k are the scale and shape parameters, here derived from [21]. Data about average number of outages in a year and average outage duration are also required to compute the total average outage duration in a year as:

Table 1
Assumed efficiency of power production technologies.

	Min	Median	Max	Source
CHP efficiency natural gas	0.33	0.34	0.35	[31]
CCGT efficiency	0.5	0.575	0.65	[32]
Efficiency of Oil Power Plant	0.31	0.365	0.42	[1]
Heavy Fuel Oil Carbon Content	–	$0.27\ \frac{kg_{CO_2}}{kWh_{th}}$	–	[33]

[1] Interview with Ghana Energy Ministry.

Table 2
Direct emissions of sources of electricity generation considered in this study.

Emissions electricity supply				
Technology	Direct Emissions $[g_{CO_2}/kWh_e]$			Source
	Min	Median	Max	
Coal [GWh]	670	760	870	[34]
Oil [GWh]	643	740	871	Elaboration from Table 1
Natural Gas [GWh]	350	370	490	[34]
Other [GWh]	530	626	910	Elaboration from Table 1

$$\overline{\text{OD}}\text{tot [h]} = \overline{\text{OD}}\ \overline{\text{NO}} \tag{10}$$

being $\overline{OD}$ the yearly average outage duration and $\overline{NO}$ the yearly number of outages. The total average time in a year in which the grid is available is thus:

$$\overline{\text{TBO}}\text{tot[h]} = 8760h - \overline{\text{OD}}\text{tot} \tag{11}$$

$$\text{t} = \text{CDF}^{-1}(r) = \lambda(-ln\ r)^{\frac{1}{k}} \tag{12}$$

The parameters $\overline{\text{TBO}}$tot and $\overline{\text{OD}}$tot are used as constraints to perform a random sampling of the above-described Weibull distributions. Sampling from Weibull distribution is made with the inversion method, i.e. calculating time samples from the inverse Weibull CDF function:

Firstly, a sampling from OD distribution is made, under the equality constraint between the sum of samples and $\overline{\text{OD}}$tot in the period of grid connection:

$$\text{t}_{\text{i OD}} = \lambda_{\text{OD}}(-\ln \text{r})^{\frac{1}{k_{OD}}} \text{ for i in 1...Nt, OD s.t. } \sum_{i}^{\text{Nti,OD}} \text{t}_{\text{OD}} = \text{ODtot Tgrid} == \text{ODtot(Tproject} - \text{Tgrid connection)} \tag{13}$$

where T_{grid}, $T_{project}$ and $T_{grid\ connection}$ are, respectively, the number of years of grid connection, the microgrid lifetime (in years) and the year at which the microgrid is connected to the national grid. Eq. (13) allows thus to obtain a set of values of outage duration whose sum respect the constraint imposed by input data in terms of total time at which the grid is not available. The same procedure is applied for TBO sampling with the constraint of same number of OD samples (i.e. same number of outages):

$$\text{t}_{\text{i, TBO}} = \lambda_{\text{TBO}}(-\ln \text{r})^{\frac{1}{k_{TBO}}} \text{ for i in 1...Nt, TBO s.t. Nt, TBO} = \text{Nt, OD} \tag{14}$$

TBO list samples are then re-scaled to match the total TBO in the period of grid connection:

$$\text{t}'_{\text{i, TBO}} = \text{t}_{\text{i, TBO}} \frac{\text{TBOtot Tgrid}}{\sum_t \text{t}_{\text{t, TBO}}} \tag{15}$$

The lists of TBO and OD samples are used to construct the grid availability matrix **G**. Since each outage event is characterized by its TBO and duration OD (both expressed in hours), **G** is constructed for each year y as:

- If $y < T_{grid\ connection}$ (i.e. microgrid not yet grid-connected), $G_{y,t} = 0\ \forall t$, being $G_{y,t}$ the element of the matrix **G** for year y and time-step t.
- If $y \geq T_{grid\ connection}$, ones and zeros in number (rounded to integers) equal, respectively, to TBO and OD of outage O are placed in series. If, for instance, the first elements of TBO and OD are equal to n and m hours, respectively, then $G1,t = 1$ for $t = 1\ldots n$ and $G1,t = 0$ for $t = n + 1\ldots n + 1 + m$.

The obtained G matrix is thus characterized by a number of columns equal to the number of years of the project, where the columns from $y =$

1 to $y = T_{grid\ connection} - 1$ are filled with null values. The underlying assumption is that connection to the grid takes place from the beginning of year $T_{grid\ connection}$.

The LP optimization problem for a grid-connected microgrid requires the definition of the variables $E^{toGrid}_{s,y,t}$ and $E^{fromGrid}_{s,y,t}$ (energy E exchanged to and from the national grid), defined on hourly time-step t of year y (for each scenario s) subject to maximum grid power constraint:

$$\begin{cases} E^{toGrid}_{s,y,t} <= Pmax, grid \cdot (1h) \\ E^{fromGrid}_{s,y,t} <= Pmax, grid \cdot (1h) \end{cases} \quad (16)$$

where $P_{max,\ grid}$ is the maximum active power exchangeable with the grid. Grid availability matrix is used to impose to 0 grid energy variables in the hours in which an outage occurs or the microgrid is not yet grid-connected:

$$\left(E^{toGrid}_{s,y,t} = 0 \text{ AND } E^{fromGrid}_{s,y,t} = 0\right) \text{ IF } G_{y,t} = 0 \quad (17)$$

$E^{toGrid}_{s,y,t}$ is imposed to be null also in the case of mono-directional grid, i.e. electricity selling not allowed:

$$E^{toGrid}_{s,y,t} = 0 \text{ IF Monodirectional\_Grid} = \text{True} \quad (18)$$

The overall microgrid energy balance constraint for each (y,t) step has been thus defined as:

$$E^{demand}_{s,y,t} = \sum_r^R E^{res}_{r,yt,t} + \sum_g^G E^{gen}_{s,g,y,t} + E^{fromGrid}_{s,y,t} + E^{batt\ dis}_{s,y,t} + E^{lost\ load}_{s,y,t} - E^{toGrid}_{s,y,t} - E^{curt}_{s,y,t} - E^{batt\ ch}_{s,y,t} \quad (19)$$

Being $E^{demand}_{s,y,t}$ the energy demand, $E^{res}_{r,yt,t}$ energy produced by the renewable source r, $E^{gen}_{s,g,y,t}$ energy produced by generator g, $E^{batt}_{s,y,t}$ energy exchanged for charging and discharging of batteries, $E^{lost\ load}_{s,y,t}$ and $E^{curt}_{s,y,t}$ the lost load and the curtailment, respectively. Each energy flow is specific to scenario *s,* year *y* and hourly time-step *t*. The investment cost for grid connection is actualized at year 1:

$$Inv^{grid}\ [\text{USD}] = \frac{Inv^{grid,km}\ Dgrid}{(1 + \text{d})^{(\text{Tgrid connection} - 1)}} \quad (20)$$

Being *d* the discount rate, *Dgrid* the grid connection distance and $Inv^{grid,km}$ the specific connection cost per km. Total actualized grid variable O&M costs and revenues are defined as:

$$O\&M^{var,grid} = \sum_{y=1}^{T_{project}} \sum_{t=1}^{8760} \frac{E^{fromGrid}_{s,y,t}\ \text{pel, purchased}}{(1 + \text{d})^y} \quad (21)$$

$$\text{R}^{grid} = \sum_{y=1}^{T_{project}} \sum_{t=1}^{8760} \frac{E^{toGrid}_{s,y,t}\ \text{pel, sold}}{(1 + \text{d})^y} \quad (22)$$

where pel, purchased and pel, sold are the buying and selling price of electricity from/to the grid, respectively. Fixed O&M costs for power line and transformer maintenance are defined as:

$$O\&M^{fixed,grid} = \sum_{y=T_{grid\ connection}}^{T_{project}} \frac{Inv^{grid,km}\ \text{Dgrid}\ x_{O\&M}}{(1 + \text{d})^y} \quad (23)$$

where $x_{grid,O\&M}$ is the fraction of grid O&M costs with respect to investment costs. All the grid cost components have been accounted in the total investment and O&M costs.

2.3. Brownfield

The new brownfield investment feature introduced in the model allows to perform the optimization of the microgrid taking into consideration the availability of technologies previously installed in the field by others. The new feature requires modification of some existing constraints and to add others.

Firstly, new constraints related to energy production of each energy source has to be included. The energy yield at each timesteps *t* by each type of renewable energy source technology *r* $E^{res}_{r,yt,t,\ u=1}$ at the first investment decision step ($u = 1$) has to be equal or higher than the energy produced by the capacity already installed on the field, as shown in Eq. (24), where $E^{res,unit}_{r,t,u=1}$ is the energy output of a single unit of each RES technology *r*, $N^{res,inst}_r$ is the number of units of *r* already installed (*inst*) on the field and $\eta^{res,inv}_r$ is the efficiency of the inverter (*inv*) connected to *r*. Regarding the generator's capacities $C^{gen,nom}_{g,u=1}$ and the battery bank's capacity $C^{batt,nom}_{u=1}$ in the first investment decision step ($u = 1$), instead, as shown by Eqs. (25) and (26), respectively, these must be equal or higher than the capacity already mounted on the field (respectively $C^{gen,inst}_g$ for each generator type *g* and $C^{batt,inst}$ for the battery bank).

$$E^{res}_{r,yt,t,\ u=1} \geq E^{res,unit}_{r,t,u=1} \cdot \eta^{res,inv}_r \cdot N^{res,inst}_r \quad (24)$$

$$C^{gen,nom}_{g,u=1} \geq C^{gen,inst}_g \quad (25)$$

$$C^{batt,nom}_{u=1} \geq C^{batt,inst} \quad (26)$$

The total investment cost (Inv^c) of each component *c* (*c* can stand for renewable energy source technologies *res*, generators *gen* and batteries *batt*) is evaluated as the actualized sum of the single investment step made at each capacity-expansion decision step *u*, with the investment cost of each technology at the first investment decision step equal to the investment cost due to the total capacity installed in the first step minus the investment cost of the capacity already connected to the microgrid, as shown in Eqs. (27)–(29) for each component:

$$Inv^{res} = \sum_{r=1}^{R} \left(\left(N^{res}_{r,u=1} - N^{res,inst}_r\right) \cdot C^{res,unit}_r \cdot U^{res}_r + \sum_{u=2}^{steps} \frac{\left[N^{res}_{r,u} - N^{res}_{r,u-1}\right] \cdot C^{res,unit}_r \cdot U^{res}_r}{(1+d)^y} \right) \quad (27)$$

$$Inv^{gen} = \sum_{g=1}^{G} \left(\left(C^{gen}_{g,u=1} - C^{gen,inst}_g\right) \cdot U^{gen}_g + \sum_{u=2}^{steps} \frac{\left[C^{gen}_{g,u} - C^{gen}_{g,u-1}\right] \cdot U^{gen}_g}{(1+d)^y} \right) \quad (28)$$

$$Inv^{batt} = \left(C^{batt}_{u=1} - C^{batt,inst}\right) \cdot U^{batt} + \sum_{u=2}^{steps} \frac{\left[C^{batt}_u - C^{batt}_{u-1}\right] \cdot U^{batt}}{(1+d)^y} \quad (29)$$

where U^c is the unitary cost of each technology *c*, C^c_u is the capacity of each component *c* at the investment decision step *u* and *d* is the discount rate.

These last modifications allow to neglect the cost of investment of the components present on the field, before the implementation of the current project, in the first investment decision step modifying the optimization process based on cost minimization approach.

Another modification is related to the salvage value (*SV*) of the installed components at the first step of investment calculated as the residual values at the end of the lifetime of the energy system, as shown in Eqs. (30) and (31), where TLT_c represents the total lifetime of each component *c* and *Y* is the total number of years of the time horizon.

$$SV^{res} = \sum_{r=1}^{R} \left(\frac{\left(N^{res}_{r,u=1} - N^{res,inst}_r\right) \cdot C^{res,unit}_r \cdot U^{res}_r \cdot \left(TLT^{res}_r - Y\right)}{TLT^{res}_r} \cdot \frac{1}{(1+d)^Y} \right) + \sum_{r=1}^{res} \left(\frac{N^{res,inst}_r \cdot C^{res,unit}_r \cdot U^{res}_r \cdot \left(TLT^{res}_r - Y^{res}_r - Y\right)}{TLT^{res}_r} \cdot \frac{1}{(1+d)^Y} \right) \quad (30)$$

$$SV^{gen} = \sum_{g=1}^{G} \left(\frac{\left(C^{gen}_{g,\ u=1} - C^{gen,inst}_{g}\right) \cdot U^{gen}_{g} \cdot \left(TLT^{gen}_{g} - Y\right)}{TLT^{gen}_{g}} \cdot \frac{1}{(1+d)^{Y}} \right) + \sum_{g=1}^{G} \left(\frac{C^{gen,inst}_{g} \cdot U^{gen}_{g} \cdot \left(TLT^{gen}_{g} - Y^{gen}_{g} - Y\right)}{TLT^{gen}_{g}} \cdot \frac{1}{(1+d)^{Y}} \right) \quad (31)$$

3. Case study and scenarios definition

The villages in question are classic examples of rural settlements with a dispersed population, a predominantly subsistence agricultural economy, few public facilities, and little private economic activities.

3.1. Mozambique

The village of Chissinguana (Table 3) is located in the Province of Sofala, District of Búzi, administrative post of Estaquinha and has 25,622 inhabitants, with 1406 at the headquarters.

The microgrid installed by FUNAE in 2018 is composed by 120 PV modules of 250 W each made of 60 Polycrystalline Silicon Cells for a total capacity of 30 kW and 144 tubular VRLA batteries of 1400 Ah and 2 V each for a total capacity of 403.2 kWh. The microgrid is equipped with 6 photovoltaic inverters with nominal AC power of 5000 W and maximum DC power of 5500 W and 3 battery inverters a nominal AC power of 6000 W and maximum DC power of 8000 W.

FUNAE deployed the microgrid after conducting a load demand study prior to construction in 2017, expecting a peak demand of roughly 10 kW. Despite the previsions made by FUNAE, the microgrid results inadequate to satisfy the energy needs of the community after just 4 years from its construction as can be seen comparing the operations of the microgrid with respect the load demand in 2021. Thanks RAMP and the information collected on the field, it's possible to evaluate the daily average load demand curve for each class of users (Households, Public Services and Productive Activities) and the aggregated daily average energy demand curve (Fig. 1), from which is possible to note a peak demand of around 35 kW, more than 3 times the peak demand evaluated by FUNAE in 2017.

Consequently, the microgrid results inadequate to meet the energy demand of the community due to an inappropriate design of the microgrid made by FUNAE. This obviously determines an important amount of lost load (yearly lost load of 88,253.3 kWh, that corresponds to 61% of the yearly total demand). Despite the important battery bank capacity installed, their usage factor (6%) is very limited due to the inability of the PV modules to recharge the batteries completely. The PV capacity installed, in fact, results too low to satisfy the demand (only 39% of the yearly total demand is covered by the PV modules) and simultaneously recharge the batteries. The absence of a fuel-fired generator is another important issue, reducing dramatically the reliability of the microgrid especially during the hours in which the PV modules are not able to produce electricity. Moreover, the system is subjected to frequent shutdown due to technical issues. In this context, the new brownfield investment feature introduced in MicroGridsPy can provide a technical solution to specifically address these issues.

Table 3
General information of the chissinguana village.

Location (Lat. Lon.)	Lat. - 20°1216.51S; Lon. - 34°0919.86E; 53 km from Muxungue village where there is the nearest national electricity grid, located in Sofala province
Population	25,622
Beneficiaries	65
Social services	Health center, School, Police office, Secretary of the locality
Productive activities	Bars, Tents, Barbershops, Tailor workshops, Mills

In order to better design the possible future interventions on the microgrid, starting from the previous load demand, different assumptions were made to evaluate the long-term evolution of the energy consumption for the remaining lifetime of the microgrid. The results of this assessment performed by means of RAMP are showed in Fig. 2.

3.2. Rwanda

For this case study the hybrid off-grid microgrid installed in Rutenderi village, in Gatsibo district, will be considered. The project, realized between 2017 and 2018 with no previously installed capacity, consists of a PV plant of 50 kW of nominal power, a lead acid battery storage system of 100 kWh and a back-up diesel generator of 50 kVA. The microgrid provides electricity through a LV distribution grid to 505 users, composed as reported in Table 4.

Since no data regarding the production from the PV system and the load profile, these have been estimated as follows. The calculation of hourly time series for PV energy production in the TMY is based on resource data by NASA POWER [36] for GHI and air temperature, provided as input to a PV performance model (additional data provided in Supplementary information SI-1).

Load demand is assessed applying the same methodology adopted by the authors in [37]. In previous work the authors developed a set of load archetypes for 5 different wealth tiers of rural households in Kenya, 4 tiers of rural health centers and of a typical primary school. The same archetypes are assumed valid for this context, given the geographical proximity and cultural similarities [38].

The archetypes composition has been thus constructed as reported in Table 5. Public institutions are assumed to have the highest demand and are considered as HHs of tier 5. The commercial activities are considered HHs of tier 4. The remaining HHs are splitted such that the computed annual energy demand is obtained (Fig. 3).

4. Results and discussion

In this section the results for the off-grid and grid-connected configurations will be presented with a particular focus on the comparison between them in terms of capacity installed, costs and direct CO_2 emissions. For Rwanda case study a greenfield investment analysis will be carried out while for the Mozambique one, the presence of already functioning microgrid makes preferable a brownfield investment approach. In each case the results for three points of the Pareto curve obtained with the multi-objective optimization will be discussed to underline the variation of the technologies capacities and costs in case of CO_2 emissions reduction.

The grid-connected configurations for the three points of the Pareto curve will be the base cases for the following sensitivity analysis on different grid parameters to evaluate how the distance from the national grid, the year of connection, the price of electricity sold from the microgrid to the national grid influence the design of the microgrids and their costs. Four different sensitivity analyses have been considered for the two case studies:

- National grid extension (only for Rutenderi): sensitivity to CO_2 emissions and grid connection distance.
- Grid-connected microgrid: sensitivity to CO_2, grid connection distance and electricity selling price.
- Grid-connected microgrid: sensitivity to CO_2 emissions and year of grid connection.
- Grid-connected microgrid: sensitivity to CO_2 emissions and reliability of the national grid.

In the following analysis only PV panels, battery bank and diesel genset will be considered for the microgrids design while wind turbines will be neglected for the very low wind speed, which characterizes the areas considered making them economically inconvenient. Moreover,

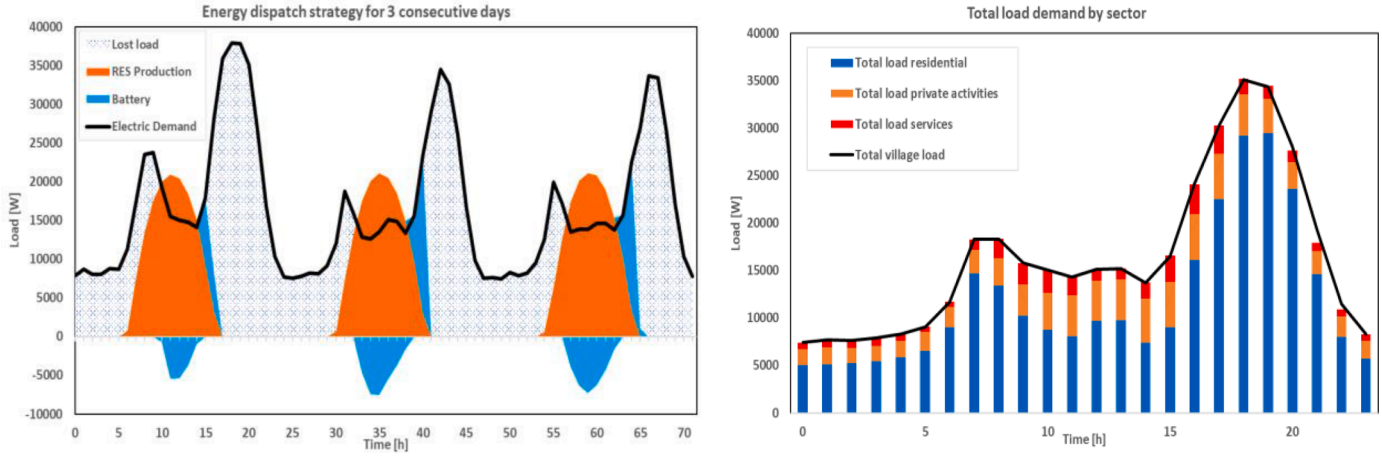

Fig. 1. Energy dispatch strategy for the existing microgrid for three consecutive days (on the left) and average daily load demand by sectors (on the right).

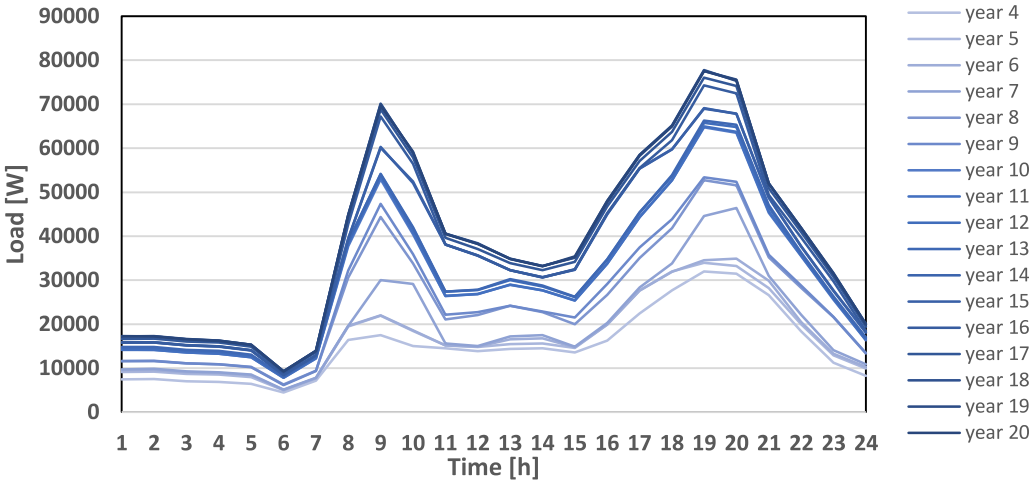

Fig. 2. Long-term evolution of load demand for Chissinguana.

Table 4
General information of the rutenderi rural area.

Location (Lat. Lon.)	Lat. −1° 33′ 56.4′′ S; Lon. 30° 21′ 3.4′′ E; 1.2 km from Point of Common Coupling (PCC) with 30 kV line
Households	457
Public institutions	7
Productive activities	36

Table 5
Assumed parameters for the construction of the total demand from archetypes.

Parameter	Value
HHs Tier 1	252
HHs Tier 2	160
HHs Tier 3	50
HHs Tier 4	36
HHs Tier 5	5
Schools	1
Hospitals Tier 2	1

only direct emissions will be considered for the difficulties in evaluating the emissions related to the construction, transportation, installation and disposal for each technology.

4.1. Chissinguana village

The microgrid that is currently set up on the field is unable to provide for the entire demand. The best strategy to fix the problems with this energy system is the brownfield investment approach. To fully meet the long-term evolving demand, this strategy results in an increase in installed capacities compared to the original asset. Particularly, the problem associated with the microgrid's low reliability is significantly diminished by the installation of a diesel genset and the already important installed battery bank capacity makes convenient the deployment of PV modules.

Fig. 4 illustrates how the multi-objective optimization can be used to compare the costs (NPC) and emissions of various solutions.

As anticipated, the significant reduction in CO_2 emissions causes a gradual rise in the NPC. With a 634.87 ton decrease in CO_2 emissions, the NPC increased by 8.9% from the ***Min_NPC*** point to the ***Intermediate*** point, but increased by 189.9% from the ***Intermediate*** point to the **Min_CO_2** point. This is primarily because, when compared to the expense of a diesel generator, cost-ineffective technologies like PV and batteries have steadily increased capacity. In particular, decreasing the CO_2 emissions, the installed capacity of PV panels and battery bank (such as the yearly average renewable penetration and battery usage)

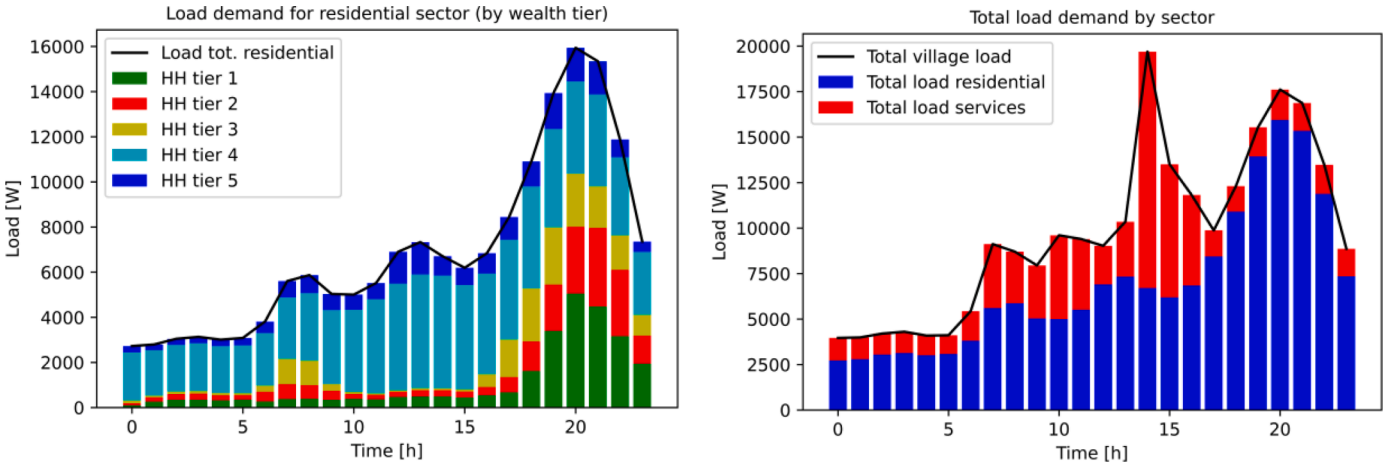

Fig. 3. Households load demand by wealth tier (left) and village total demand by sector (right).

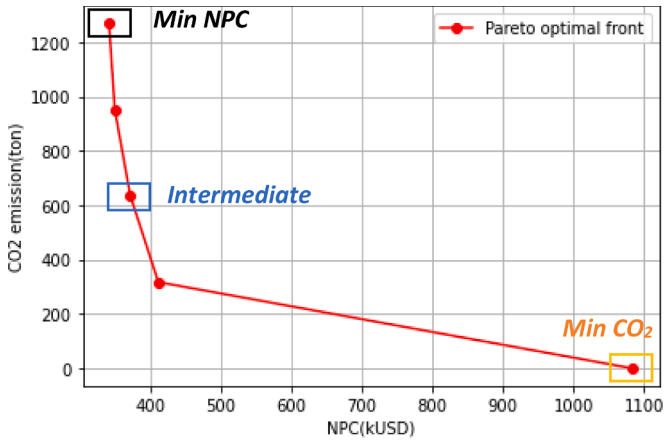

Fig. 4. Pareto frontier for off-grid configuration.

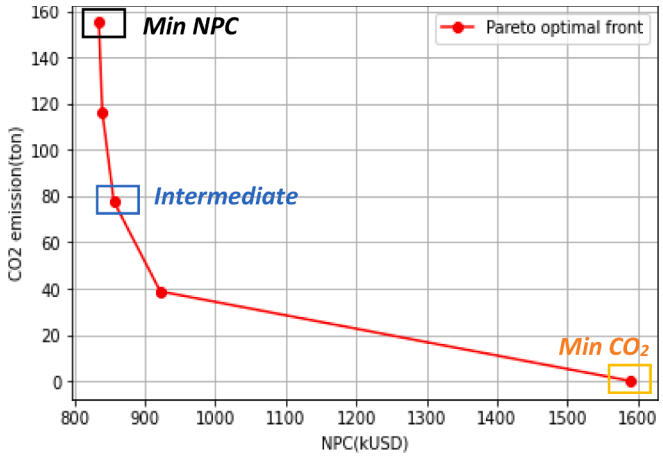

Fig. 5. Pareto frontier for grid-connected configuration.

increases in favour of diesel genset capacity (such as the yearly average genset share over the total production) in order to limit the emissions related to fuel consumption. The absence of diesel genset in the **Min_CO$_2$** point allows to completely cut off the CO_2 emission with a cost for the CO_2 avoided equal to 585.1 USD/tonCO_2 Table 6.

Connecting the microgrid to the national grid, as part of the brownfield investment approach, leads to a strong increase of the NPCs for each point of the Pareto curve (Fig. 5), mainly due to the prohibitive investment cost for the extension of the national grid from the nearest point situated at 53 km. On the other side, the CO_2 emissions are strongly decreased thanks to the reduction of diesel consumption.

The main grid connection determines a rough reduction of the installed genset capacity in the microgrid compared to off-grid configurations, but the reduction of the average annual genset share over total production is more significant (for instance, in the ***Min_NPC*** point, the average annual genset share is 0.04% with respect the 27.05% in the off-grid case). Because it is less cost-effective than electricity from the national grid (yearly average grid usage equals 53.70% in the ***Min_NPC*** point), the diesel generator is only used when the main grid is down.

Table 6
Capacity installed in off-grid configuration.

Component	*Unit*	*Min NPC*	*Intermediate*	*Min CO_2*
PV panels	kW	119.03	157.69	721.22
Battery bank	kWh	464.61	708.32	1177.01
Diesel genset	kW	34.86	29.42	0

Table 7
Installed capacity in grid-connected configuration.

Component	*Unit*	*Min NPC*	*Intermediate*	*Min CO_2*
PV panels	kW	142.22	156.94	721.23
Battery bank	kWh	403.20	436.17	1176.94
Diesel genset	kW	27.43	24.68	0

Additionally, as shown in Table 7, the opportunity to sell the electricity generated by the microgrid to the national grid determines an increase in the PV installed capacity, determining an important flow of revenues, particularly in the first years, and drastically reducing the curtailment (in the ***Min_NPC*** point, the yearly average curtailment is 0.10% versus the 9.26% in the off-grid case). Finally, the connection to the national grid limits the battery usage and, consequently, the need of important battery bank capacity like in the previous case for the ***Min_NPC*** and ***Intermediate*** point.

As for the off-grid case, minimizing the CO_2 emissions results in a complete avoidance of the embedded emissions to the main grid's electricity as well as the direct emissions associated to fuel consumption. Consequently, the microgrid configuration in the **Min_CO$_2$** point remains unaltered between the off and on-grid cases, with the electricity produced in excess by the microgrid sold to the main grid but insufficient to cover the important grid investment cost.

This initial comparison of grid-connected and off-grid configurations shows that there is no cost-effective alternative to the off-grid design

when the main grid is expanded to reach the microgrid, which is located 53 km from the nearest national grid point. However, assuming to make the grid-connected configuration a competitive alternative, it is conceivable to identify a break-even distance for each examined point of the Pareto curve that makes the NPC of the grid-connected case equal to that of the off-grid scenario (Table 8).

Each point on the Pareto curve has a different break-even distance based on the NPC of the grid-connected and off-grid configurations. Since the ***Intermediate*** point has the smallest difference, a greater distance can be accepted to maintain the competitiveness of the grid-connected design.

4.1.1. Sensitivity on fuel price

These days, the global rise in fuel prices is having a significant impact. Fuel (particularly diesel) is continuously utilized in this type of application to power fuel-fired gensets that significantly boost the energy system's reliability by meeting peak energy demand or during the night.

Because of this, it could be useful to conduct a sensitivity analysis on fuel prices to determine how a potential rise of 10%, 20%, or 25% in fuel prices might affect the development and operation of an off-grid energy system.

In Table 9, only the point at minimum NPC is taken into consideration. Due to the rising cost of fuel, genset capacity is being roughly reduced in favour of PV panels and batteries, which are required to meet a larger portion of the night load in place of genset production. Naturally, this results in greater expenditures, mostly in the form of higher investment costs, but it also results in a decrease in CO_2 emissions due to fuel use and a decline in the average annual genset share.

Fuel price fluctuations in the grid-connected example have minimal effects on system size and expenses. This is because the diesel generator is generally used briefly and is typically only employed in cases of national grid failure. As a result, the microgrid's energy plan dispatch is unaffected continuously by fuel price increases, and NPC growth is not very noteworthy.

4.1.2. Sensitivity on distance and selling price

The distance of the microgrid from the nearest point of the main grid and the price at which any excess electricity generated by the microgrid might be sold to the national authority (electricity selling price) are two crucial elements in the description of the connection of the national grid to the off-grid system. These two factors have an impact on the microgrid's size, energy dispatch strategy, and subsequently, associated costs and emissions.

For each Pareto point, Fig. 6 shows the linear variation of the NPC in relation to the distance between the microgrid and the nearest national grid point. The NPC modification based on the selling price of electricity produces more interesting results. The NPC increases progressively as expected when it moves from an electricity selling price equal to the electricity buying price (100% case) to the no selling case.

At the same way, the variation of the CO_2 emissions can be observed in Fig. 7, where a different trend can be noticed with respect the NPC one. The distance fluctuation has no impact on CO_2 emissions since it has no bearing on the microgrid's energy dispatch strategy. The lowest emissions are found at the point when the price of electricity sold is equal to 50% of the price of power purchased, followed by the point where no electricity is sold and the point where the price is 100%. Furthermore, regardless of the price at which power is sold, emissions are always zero for the alternatives with the lowest CO_2 emissions. The reasons of these trends can be better explained analysing the results for a specific distance, which are showed in Table 10.

Table 8
Break-even distances for each point of the Pareto curve.

	Break-even distance (km)
Min NPC	16.09
Intermediate	16.76
Min CO_2	15.18

Table 9
Variation of system size, CO_2 emissions and NPC according to fuel price increment.

Min NPC point					
Component	*Unit*	*Base case*	*10% case*	*20% case*	*25% case*
PV panels	kW	119.03	123.83	128.42	131.13
Battery bank	kWh	464.61	486.84	511.59	529.75
Diesel Genset	kW	34.86	33.34	32.74	32.32
Objectives	*Unit*	*Base case*	*10% case*	*20% case*	*25% case*
NPC	kUSD	341.22	355.91	369.76	376.18
CO_2 emissions	ton	1269.75	1188.60	1110.01	1060.64

So first of all, it is possible to see that the larger NPC in the no-selling case due to the lack of grid profits is the only difference for the points at minimum CO_2. The PV and BESS capacities significantly rise in the 50% case in the ***Intermediate*** and ***Min_NPC*** points (with respect the no selling case and the 100% case), significantly reducing the energy supplied by the grid. The higher PV capacity installed determines a greater amount of electricity sold, even though the power selling price is lower than in the 100% case. Because of the considerable increase in the amount of electricity sold and consequent rise in associated revenues, it is still convenient to oversize the microgrid and produce more electricity than in the 100% case. This is because the increase in investment costs is less significant than the decrease in variable expenses. In the 50% scenario, the larger share of PV generation enables a reduction in the grid share and diesel genset capacity (and, as a result, in the grid cost associated with acquiring power from the grid), resulting in fewer emissions compared to the other two options. As there is no way to cut the variable cost through the sale of energy, the no selling situation instead tends to install lesser capacity, decreasing the investment cost.

4.1.3. Sensitivity on year of connection

The year that the microgrid is connected to the national grid has an impact on both the system's size and energy dispatch strategy. Depending on the Pareto curve point taken into consideration, connecting the microgrid to the national grid after ten years from the off-grid system's construction results in different outcomes.

Comparing the configurations for year 10 of connection with respect year 1 Fig. 8:

- At ***Min_NPC*** point, despite the grid's absence for the first nine years, the PV capacity and diesel genset capacity are both lowered, but overall their annual average share of total production is increased (respectively, 70.13% versus 65.34% and 10.76% versus 0.04%) and also batteries play a larger role (19.21% versus 1.45%). Despite the decrease in investment costs, the sharp rise in fuel and battery replacement costs, as well as the inability to sell surplus power in the early years (cutting curtailment), leads in a moderate rise in NPC and CO_2 emissions.
- At ***Intermediate*** point, connecting the microgrid at the year 10 leads, instead, to an increase of the PV and battery bank capacities in favour of the diesel genset. The diesel genset share is still higher (3.98% vs 0.03%) increasing the fuel cost, which when combined with reduced power sales revenues results in a rough increase of the NPC despite the lower actualized investment cost. In terms of emission the connection at the year 10 determines a total CO_2 emissions three times higher than the case with the year of connection 1, mainly due to the important increase of fuel consumption in the first years.
- Finally, at **Min_CO_2** point, the microgrid to the main grid at the year 10 results in a smaller PV capacity installed in order to reduce the investment cost taking into account the lack of potential earnings in

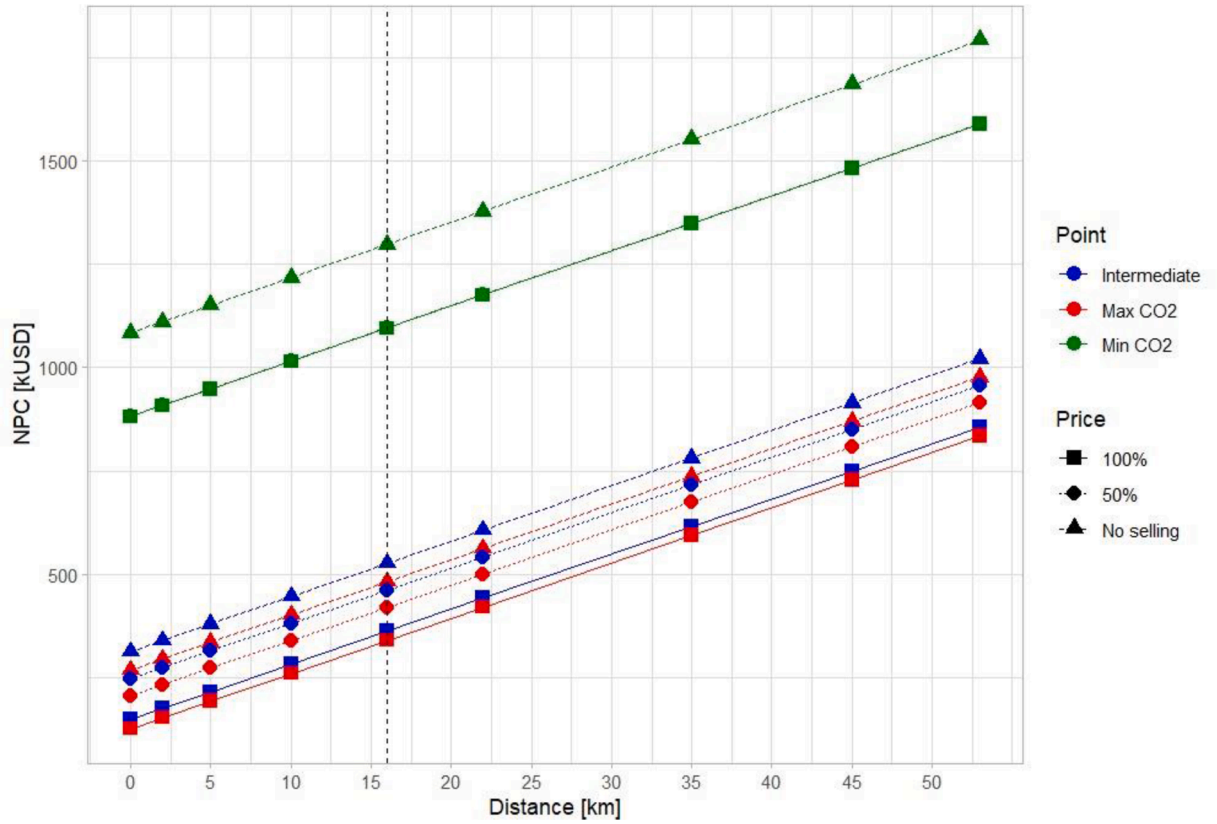

Fig. 6. Net Present Cost as function of grid distance and electricity selling price for maximum CO_2, minimum CO_2 and intermediate point (Chissinguana microgrid). The black dashed line represents the break-even distance for the intermediate point at 100% selling price.

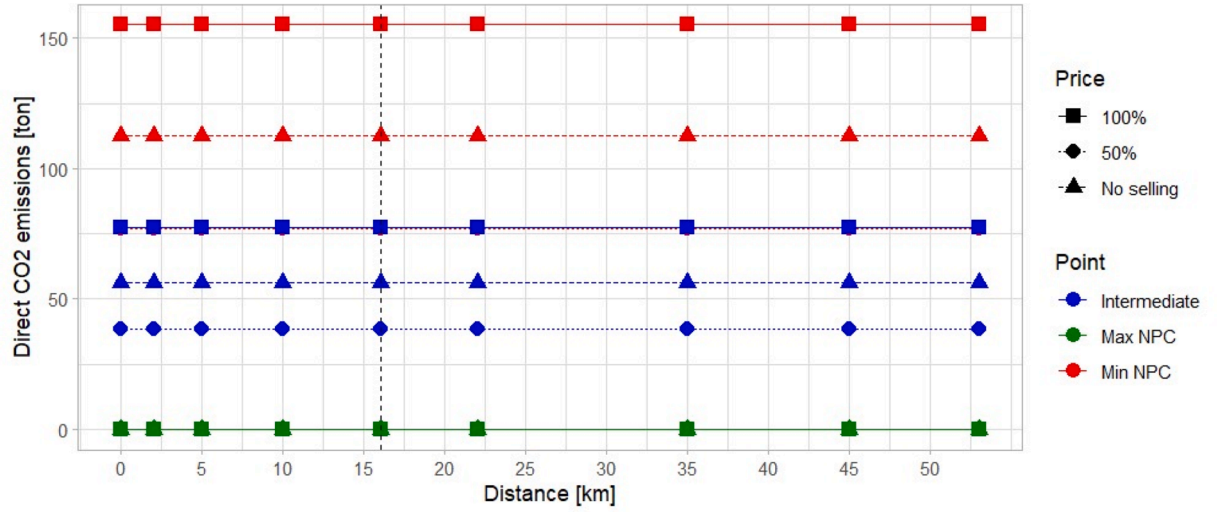

Fig. 7. Direct CO_2 emissions as function of grid distance and electricity selling price for maximum NPC, minimum NPC and intermediate point (Chissinguana microgrid).

the initial years. Overall, given the lower NPC in this situation, primarily because of the lower investment cost, it ends up being more convenient to connect the microgrid to the main grid at year 10.

4.2. Rutenderi village

Optimization results for the off-grid configuration show a moderate increase of NPC (Fig. 9) shifting from ***Min_NPC*** point to the ***Intermediate*** (+3 kUSD). The achieved 50% reduction in direct CO_2 emissions is obtained with additional PV and battery capacity (Table 11) and lower diesel consumption (−5%). In the **Min_CO_2** point further PV and battery capacity is added and diesel genset is excluded, leading to a much higher NPC (82 kUSD) and no direct emissions.

Grid-connected configuration, at 1:1 selling/buying price ratio, shows a significantly lower NPC (Fig. 10) compared to off-grid for both ***Min_NPC*** and ***Intermediate*** points. This is due firstly to the use of cheaper national grid electricity instead of batteries to satisfy the demand in no PV production periods and secondly to the possibility of

Table 10
Capacities installed and main microgrid parameters with 2 km of distance.

	Min CO_2			*Intermediate*			*Min NPC*		
	100%	*50%*	*NO*	*100%*	*50%*	*NO*	*100%*	*50%*	*NO*
PV panels (kW)	721.23	721.24	721.22	156.94	211.49	144.66	142.22	208.98	98.33
BESS (kWh)	1176.94	1176.89	1177.01	436.17	658.36	624.79	403.20	403.20	403.20
Diesel Genset (kW)	0.00	0.00	0.00	24.68	9.91	14.10	27.43	25.43	29.12
	Min CO_2			*Intermediate*			*Min NPC*		
	100%	*50%*	*NO*	*100%*	*50%*	*NO*	*100%*	*50%*	*NO*
NPC (kUSD)	907.93	907.93	1110.90	174.15	273.40	339.28	152.82	232.23	294.72
CO_2 emissions (ton)	0.00	0.00	0.00	77.58	38.42	56.23	155.17	76.85	112.46
Grid cost (kUSD)	0.00	0.00	0.00	88.80	39.67	59.77	206.37	89.03	129.60
Grid revenues (kUSD)	360.19	275.37	0.00	160.65	135.08	0.00	251.75	155.99	0.00

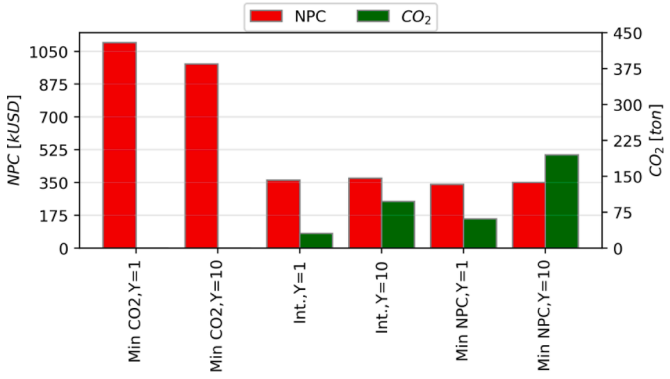

Fig. 8. NPC (red) and direct CO_2 emissions (green) for year 1 and 10 of connection to the grid, for the three considered Pareto curve points.

selling electricity to the grid. In ***Min_NPC*** point indeed no batteries are installed (Table 12) and diesel genset is sized as back-up for grid outages. In the ***Intermediate*** point, both grid electricity and batteries are used to satisfy the night-time demand, with outages covered either by batteries or diesel genset depending on the available SOC. At **Min_CO_2**, electricity is only sold to the grid relying on large PV and battery capacity.

Assumed input data for off-grid and grid-connected configurations are available in Supplementary information SI-1.

4.2.1. National grid extension

National grid extension is considered to evaluate the profitability of exploiting the national power grid without the installation of a microgrid. NPC for grid extension Fig. 11) is a linear function of connection distance (Eqs. (20) and ((23)). The electricity from the national grid is used to supply the demand except for outage periods, where batteries (***Min_CO_2***) or the diesel generator (***Min_NPC***) are employed. For the **Min_CO_2** point the achievable reduction in emissions is negligible (- 4 ton) compared to a large increase in investment and fixed costs for large battery capacity (+97 kUSD). The break-even PCC distance, calculated with respect to the off-grid system in the ***Intermediate*** point, is lower (1.18 km) than the actual connection distance thus grid extension results to be less profitable than the off-grid solution.

4.2.2. Sensitivity to battery bank capital cost

An increase in battery bank capital cost may be determined by fluctuations in the price of components raw materials such as lithium. The recent increase in lithium price is considered a potential driver for the rise of lead-acid batteries price as well [39]. A sensitivity analysis has been thus performed for the off-grid configuration considering 3

Table 11
Comparison of system size in the off-grid configuration for three Pareto curve points.

Component	*Min NPC*	*Intermediate*	*Min CO_2*
PV capacity [kW]	58.5	65.6	93
Battery capacity [kWh]	207.1	221.3	356
Diesel genset capacity [kW]	3.9	3.4	0

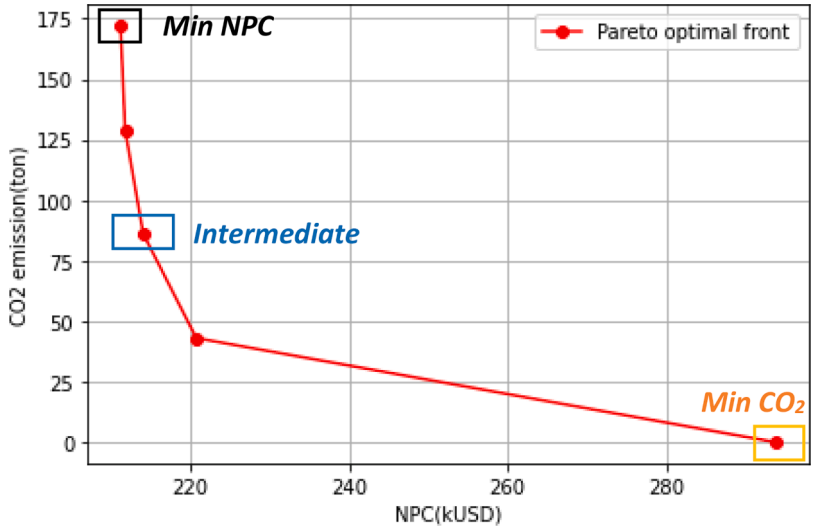

Fig. 9. Pareto frontier for off-grid configuration (Rutenderi microgrid).

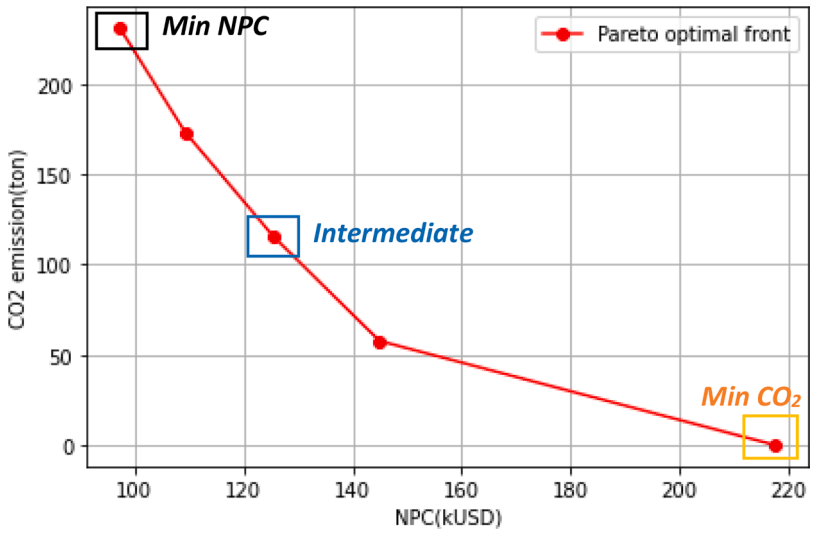

Fig. 10. Pareto frontier for grid-connected configuration (Rutenderi microgrid).

Table 12
Comparison of system size in the grid-connected configuration (1:1 selling/buying price ratio) for three Pareto curve points.

Component	*Min NPC*	*Intermediate*	*Min CO_2*
PV capacity [kW]	57.4	66	93
Battery capacity [kWh]	0	106.1	356.2
Diesel genset capacity [kW]	22.6	5.3	0

percentage increments in battery cost. Results for the **Min_CO_2** point are reported in Table 13. Optimal PV installed capacity increases and battery capacity decreases until 20% growth in battery cost, after which components size remains fixed. This occurs since batteries are progressively less used to support minimum PV production hours (at sunrise and sunset) and the gap is filled with additional PV capacity, until saturation.

In ***Min_NPC*** and ***Intermediate*** points, higher battery cost leads instead to larger deployment of diesel genset and thus higher CO_2 emissions.

4.2.3. *Grid-connected: sensitivity to distance and selling price*

For different combinations of PCC distance and selling price, the NPC results (Fig. 12) show how selling electricity to the grid, even at 50% of buying price, leads to a 14% reduction (average for the 3 CO_2 points) of NPC compared to only-purchase connection. Selling price determines different system sizes (Table 14) and CO_2 emissions (Fig. 13): in ***Min_NPC*** at 1:2 selling/buying price ratio the optimal PV capacity is almost 5 times than in no-selling case, due to the profitability of oversizing the PV system and selling to the grid. Shifting from 1:2 to 1:1 price ratio optimal PV capacity is reduced by 40% while the revenues from electricity selling remain constant, i.e. electricity sold to the grid is halved. CO_2 emissions, at fixed Pareto point, are constant with distance (no changes in system size and dispatch) and almost constant for different price ratios: the minimum is obtained at 50% owing to the maximum PV capacity installed.

4.2.4. *Grid-connected: sensitivity to year of connection*

The year of connection to the national grid strongly influences system costs and configuration. The NPC, in case of connection at half of

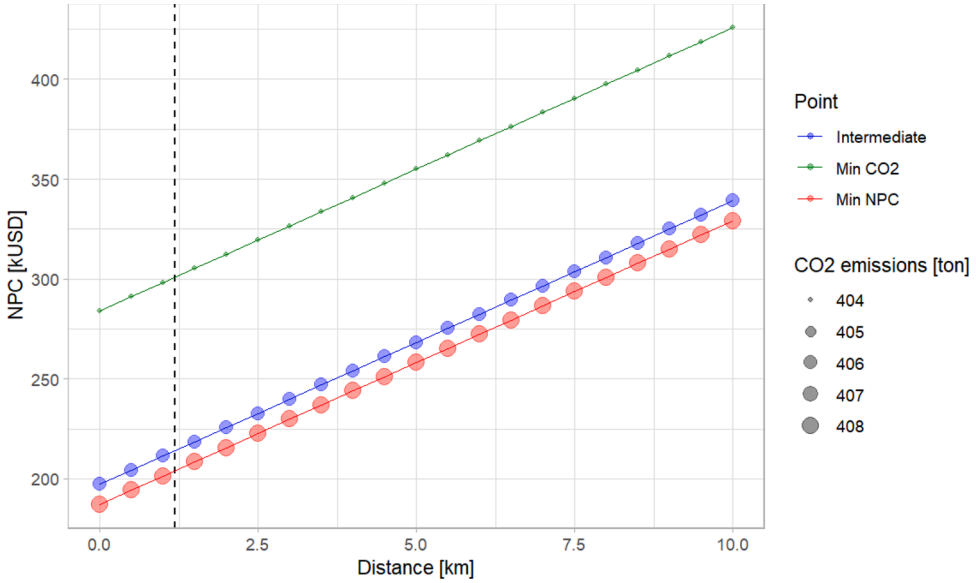

Fig. 11. Net Present Cost as function of connection distance for the 3 selected Pareto curve points (**Min_CO_2** emissions, **Intermediate, Min_NPC**) in the case of national grid extension. The dashed line represents the break-even distance with the off-grid system for the **Intermediate** point.

Table 13
Variation of system size, CO_2 emissions and NPC according to fuel price increment.

Min CO_2 point					
Component	*Unit*	*Base case*	*10% case*	*20% case*	*25% case*
PV panels	kW	93	103.1	126	126
Battery bank	kWh	356	324.4	256.7	256.7
Diesel Genset	kW	0	0	0	0
Objectives	*Unit*	*Base case*	*10% case*	*20% case*	*25% case*
NPC	kUSD	293.7	314.9	333.1	341.8

microgrid lifetime (year 10), results always higher than at the beginning of lifetime (Fig. 14). In the ***Min_NPC*** point, the optimization must account indeed for a period of off-grid operation, in which installing a storage system should be more convenient than diesel genset (Table 11) and a period of grid-connected operation, where diesel genset is more convenient than batteries (Table 12). The dispatch is thus characterized by the reliance on PV+batteries for the first 10 years of operation and on PV+grid in the remaining lifetime, with grid outages covered by installed batteries. Total CO_2 emissions are instead higher connecting at the first year due to larger utilization of grid electricity. The same holds for the ***Intermediate*** CO_2 point, which only differentiates for the smaller deployment of diesel. In the **Min_CO_2** point the difference in NPC is small and due only to electricity selling, which in the case of year 10-connection leads to higher PV and battery optimal capacity.

5. Conclusions

The goal of this paper was to propose a new set of features to an existing microgrid sizing tool in order to obtain a methodology up to date with the new challenges that the sector is facing. From an already established methodology of multi-year capacity expansion optimization of off-grid energy systems, able to work with two-stage stochastic optimization, three different implementations are carried out.

In order to include in the sizing logic the direct CO_2 emissions related with the power generation of the microgrid, and allow the developers to consider a variety of options ranging from the least cost to the net-zero direct emission option, a two-objective optimization is introduced.

The multi-objective optimization allowing for the evaluation of the lowest cost option, lowest CO2 options and an equilibrium between the two provides a policymaker both on national and local levels with a wider array of options and solutions. Such a flexibility of the model not only can help solving urgent problems and satisfy basic needs of the population, namely access to energy, but applying Maslow's hierarchy of needs to energy sector, once these needs are covered, the development process and the societal challenges like climate change may incite new demands, like conscious energy consumption and environmental

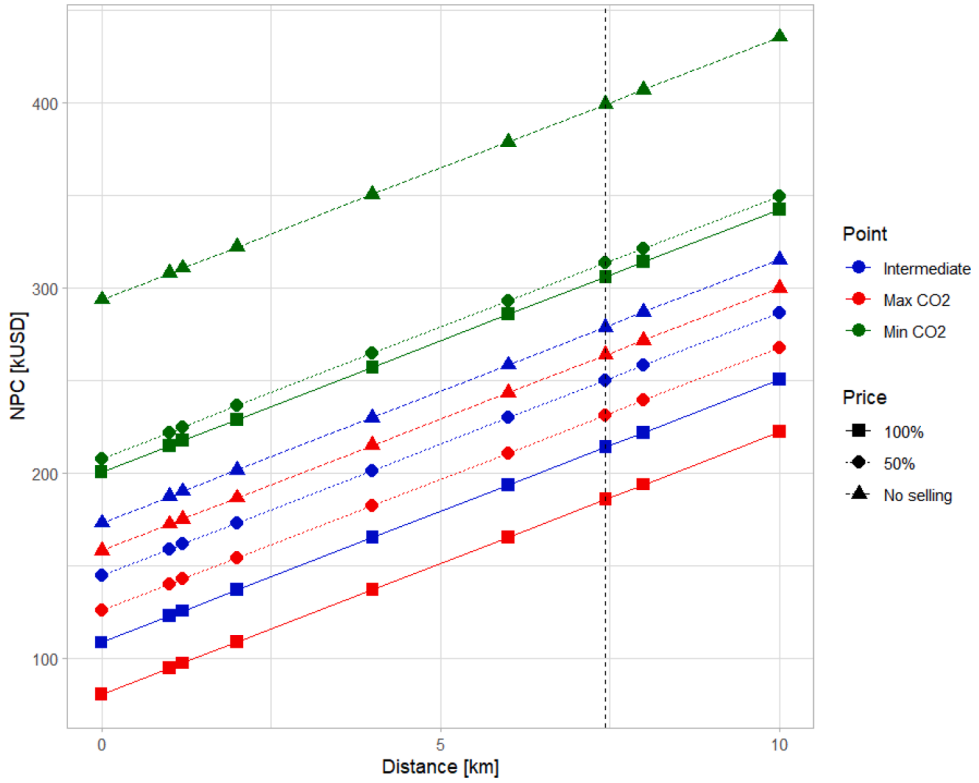

Fig. 12. Net Present Cost as function of grid distance and electricity selling price for **Min_NPC, Min_CO_2** and **Intermediate** point (Rutenderi microgrid). The black dashed line represents the break-even distance for the **Intermediate** point at 100% selling price.

Table 14
Comparison of the optimal system size with no selling and selling price equal to 100% buying price, for the **Min_NPC** point.

	Min CO_2			*Intermediate*			*Min NPC*		
Component	*100%*	*50%*	*NO*	*100%*	*50%*	*NO*	*100%*	*50%*	*NO*
PV panels (kW)	93	93	93	66	96	42.2	57.4	95.3	21.9
BESS (kWh)	356	356	356	106.1	107.3	118.6	10.3	0	0
Diesel Genset (kW)	0	0	0	5.3	5.2	4.6	20.6	22.6	22.6

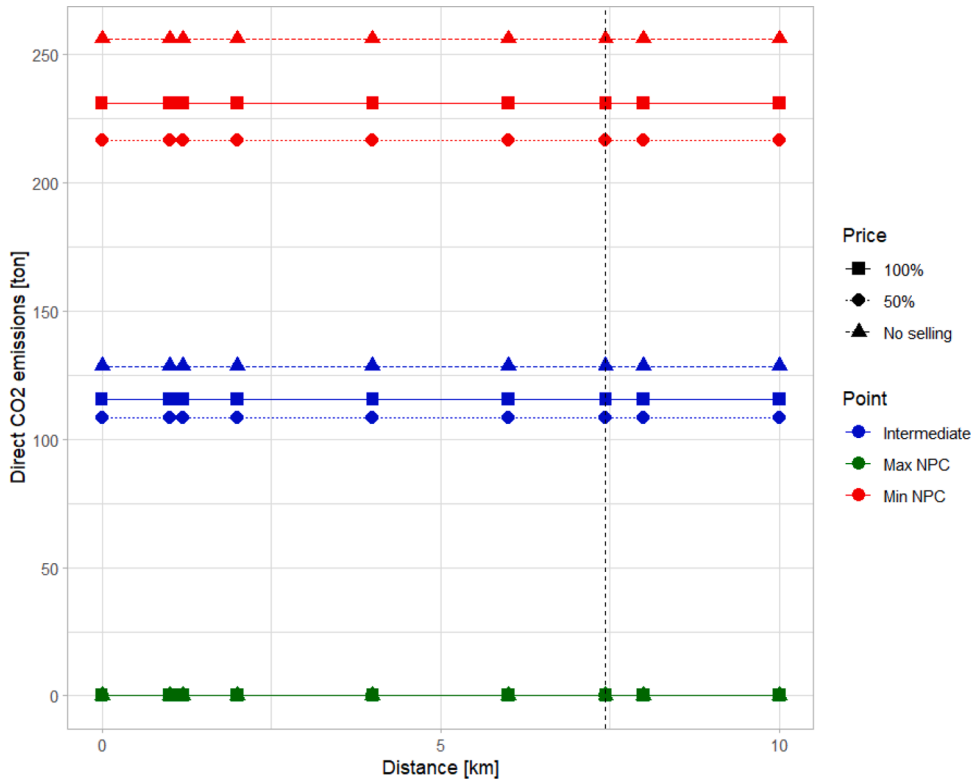

Fig. 13. Direct CO_2 emissions as function of grid distance and electricity selling price for **Min_CO_2**, **Min_NPC** and **Intermediate** point (Rutenderi microgrid).

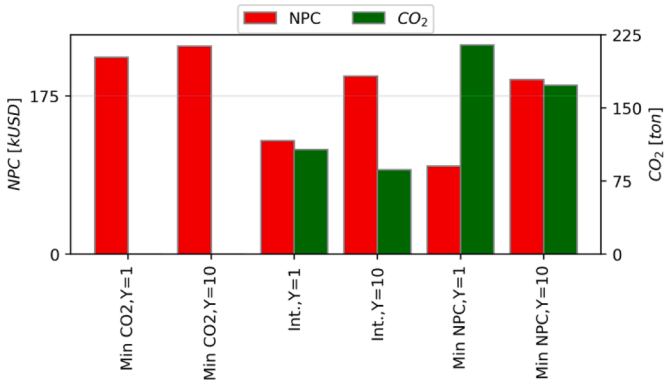

Fig. 14. NPC (red) and direct CO_2 emissions (green) for year 1 and 10 of connection to the grid, for the three considered Pareto curve points.

awareness. Thus, the possibility to choose or balance between cost and CO2 emissions (a crucial factor for the system's sustainability and the ongoing energy transition), gives a policymaker a valuable tool for a medium- and long-term strategic planning in line with the 2030 UN Sustainable Development Goals and the objectives of the African Union's Agenda 2063 able to guarantee long-term sustainability and resilience of the energy system and within communities.

Given the latest trend in minigrid development that saw the come to the market of a new generation of minigrids, able to connect to the national grid, it is important for planners and developers to take into account this possible change in the structure of the operating system during its lifetime. For this reason the possibility to account for the connection of the off-grid system to the main grid is added to the tool. In this way it is possible to plan the installation of the grid taking into account that at a certain point of the operating lifetime a new energy source will become available. In addition to that is possible to model both mono and bidirectional grid connections, and specific grid reliability, different for different parts of the African continent.

Lastly, another issue often encountered in off-grid system sizing is the presence of already existing systems, in this situation it is necessary to plan an expansion of the existing system in order to meet the new needs emerged from the community, the so-called brownfield sizing. For this reason the possibility to perform brownfield optimization has been developed. This represents an important advancement under the practical point of view, especially for practitioner involved in the field, that many times face this situation.

Data availability

In accordance with the latest trends of open science and open source modelling [40], the release of the model is available at: https://github.com/SESAM-Polimi/MicroGridsPy-SESAM/releases/tag/v0.2.0.

Funding

This work is developed in the framework of the SETaDiSMA project. The SETaDiSMA project is part of the LEAP-RE Program. LEAP-RE has received funding from the European Union's Horizon 2020 Research and Innovation Program under Grant Agreement 963530.

Declaration of Competing Interest

The authors declare that they have no known competing financial interests or personal relationships that could have appeared to influence the work reported in this paper.

Data availability

Data is openly available alongside the source code of the model on GitHub as reported in Data Availability section of the manuscript.

Supplementary materials

Supplementary material associated with this article can be found, in the online version, at doi:10.1016/j.rset.2023.100053.

References

[1] World Bank Group, COP26 Climate Brief - Energy Transition and Universal Access, World Bank, 2021. Consultato: 31 maggio 2022. [Online]. Disponibile su, https://thedocs.worldbank.org/en/doc/e7fbd4099b9a937ff2d775e0f38aaa98-0020012021/original/COP26-ClimateBriefs-EnergyTransition-Final-2610.pdf.

[2] IEA, IRENA, UNDS, T. W. Bank, e WHO, Tracking SDG7: The Energy Progress Report, International Bank for Reconstruction and Development, 2021 [Online]. Disponibile su, www.worldbank.org.

[3] IEA, Africa Energy Outlook 2019, IEA, 2019.

[4] S. Mandelli, J. Barbieri, R. Mereu, E. Colombo, Off-grid systems for rural electrification in developing countries: definitions, classification and a comprehensive literature review, Renew. Sustain. Energy Rev. 58 (2016) 1621–1646, https://doi.org/10.1016/j.rser.2015.12.338.

[5] ESMAP, Mini Grids for Half a Billion People: Market Outlook and Handbook for Decision Makers, The World Bank, 2019. ESMAP Technical Report; 014/19 [Online]. Disponibile su: https://openknowledge.worldbank.org/handle/10986/31926.

[6] International Renewable Energy Agency (IRENA), Policies and Regulations for Renewable Mini-Grids, International Renewable Energy Agency (IRENA), 2018.

[7] IRENA, Innovation Outlook Mini-Grids, IRENA, 2016 [Online]. Disponibile su, www.irena.org%0Awww.irena.org/publications.

[8] ESMAP, Mini Grids and the Arrival of the Main Grid: Lessons from Cambodia, ESMAP, Sri Lanka, and Indonesia, 2018.

[9] J. Peters, M. Sievert, M.A. Toman, Rural electrification through mini-grids: challenges ahead, Energy Policy 132 (May) (2019) 27–31, https://doi.org/10.1016/j.enpol.2019.05.016.

[10] B. Akbas, A.S. Kocaman, D. Nock, P.A. Trotter, Rural electrification: an overview of optimization methods, Renew. Sustain. Energy Rev. 156 (2022), https://doi.org/10.1016/j.rser.2021.111935.

[11] R. Dufo-López, I.R. Cristóbal-Monreal, J.M. Yusta, Optimisation of PV-wind-diesel-battery stand-alone systems to minimise cost and maximise human development index and job creation, Renew. Energy 94 (2016) 280–293, https://doi.org/10.1016/j.renene.2016.03.065.

[12] M. Petrelli, D. Fioriti, A. Berizzi, C. Bovo, D. Poli, A novel multi-objective method with online Pareto pruning for multi-year optimization of rural microgrids, Appl. Energy 299 (2021), https://doi.org/10.1016/j.apenergy.2021.117283.

[13] Website: HOMER - hybrid renewable and distributed generation system design software. [online] https://www.homerenergy.com/index.html (accessed 7 June2022).

[14] Website: The difference between greenfield vs. brownfield investments, *Investopedia*. [online] https://www.investopedia.com/ask/answers/043015/what-difference-between-green-field-and-brown-field-investment.asp (accessed 15 june 2022).

[15] I. Alsaidan, W. Gao, A. Khodaei, Optimal design of battery energy storage in stand-alone brownfield microgrids, in: Proceedings of the North American Power Symposium (NAPS), NAPS, 2017, pp. 1–6, https://doi.org/10.1109/NAPS.2017.8107245.

[16] M. Jaszczur, Q. Hassan, P. Palej, J. Abdulateef, Multi-Objective optimisation of a micro-grid hybrid power system for household application, Energy 202 (2020), 117738, https://doi.org/10.1016/j.energy.2020.117738.

[17] N. Stevanato, F. Lombardi, E. Colmbo, S. Balderrama, S. Quoilin, Two-stage stochastic sizing of a rural micro-grid based on stochastic load generation, in: Proceedings of the IEEE Milan PowerTech, PowerTech 2019, IEEE, 2019, https://doi.org/10.1109/PTC.2019.8810571.

[18] N. Stevanato, et al., Long-term sizing of rural microgrids: accounting for load evolution through multi-step investment plan and stochastic optimization, Energy Sustain. Dev. 58 (2020) 16–29, https://doi.org/10.1016/j.esd.2020.07.002.

[19] N. Stevanato, L. Rinaldi, S. Pistolese, S.L.B. Subieta, S. Quoilin, E. Colombo, Modeling of a village-scale multi-energy system for the integrated supply of electric and thermal energy, Appl. Sci. 10 (21) (2020) 1–20, https://doi.org/10.3390/app10217445.

[20] S. Balderrama, F. Lombardi, F. Riva, W. Canedo, E. Colombo, S. Quoilin, A two-stage linear programming optimization framework for isolated hybrid microgrids in a rural context: the case study of the "El Espino" community, Energy 188 (2019).

[21] F.S. Kebede, J.C. Olivier, S. Bourguet, M. Machmoum, Reliability evaluation of renewable power systems through distribution network power outage modelling, Energies 14 (11) (2021), https://doi.org/10.3390/en14113225.

[22] G.Chiandussi, M. Codegone, S. Ferrero, F.E. Varesio, Comparison of multi-objective optimization methodologies for engineering applications, Computers & Mathematics with Applications 63 (5) (2012), doi:10.1016/j.camwa.2011.11.057.

[23] Y. Cui, Z. Geng, Q. Zhu, Y. Han, Review: multi-objective optimization methods and application in energy saving, Energy 125 (2017) 681–704, https://doi.org/10.1016/j.energy.2017.02.174.

[24] J. Martínez-Gomez, J. Peña-Lamas, M. Martín, J.M. Ponce-Ortega, A multi-objective optimization approach for the selection of working fluids of geothermal facilities: economic, environmental and social aspects, J. Environ. Manag. 203 (2017) 962–972, https://doi.org/10.1016/j.jenvman.2017.07.001.

[25] L. Li, H. Mu, N. Li, M. Li, Economic and environmental optimization for distributed energy resource systems coupled with district energy networks, Energy 109 (2016) 947–960, https://doi.org/10.1016/j.energy.2016.05.026.

[26] J. Zhong, T.E. Yu, C.D. Clark, B.C. English, J.A. Larson, C.L. Cheng, Effect of land use change for bioenergy production on feedstock cost and water quality, Appl. Energy 210 (2018) 580–590, https://doi.org/10.1016/j.apenergy.2017.09.070.

[27] C. Cambero, T. Sowlati, Incorporating social benefits in multi-objective optimization of forest-based bioenergy and biofuel supply chains, Appl. Energy 178 (2016) 721–735, https://doi.org/10.1016/j.apenergy.2016.06.079.

[28] D. Zhang, S. Evangelisti, P. Lettieri, L.G. Papageorgiou, Optimal design of CHP-based microgrids: multiobjective optimisation and life cycle assessment, Energy 85 (2015) 181–193, https://doi.org/10.1016/j.energy.2015.03.036.

[29] Website:Data tables – data & statistics, *IEA*. [online] https://www.iea.org/data-and-statistics/data-tables (accessed 16 May2022).

[30] Website: IRENA, Country profiles, */statistics/view-data-by-topic/renewable-energy-balances/country-profiles*. [online] https://www.irena.org/Statistics/View-Data-by-Topic/Renewable-Energy-Balances/Country-Profiles (accessed 16 may 2022).

[31] IEA, Technology Brief E04 - Combined Heat and Power, IEA, 2022. Consultato: 20 maggio [Online]. Disponibile su, https://iea-etsap.org/E-TechDS/PDF/E04-CHP-GS-gct_ADfinal.pdf.

[32] IEA, Technology Brief E02 - Gas-Fired Power, IEA, 2022. Consultato: 20 maggio [Online]. Disponibile su, https://iea-etsap.org/E-TechDS/PDF/E02-gas_fired_power-GS-AD-gct_FINAL.pdf.

[33] Website:Combustion of fuels - carbon dioxide emission. [online] https://www.engineeringtoolbox.com/co2-emission-fuels-d_1085.html (consultato 16 maggio 2022).

[34] Intergovernmental Panel on Climate Change, Climate Change 2014 Mitigation of Climate Change: Working Group III Contribution to the Fifth Assessment Report of the Intergovernmental Panel on Climate Change, Cambridge University Press, Cambridge, 2014, https://doi.org/10.1017/CBO9781107415416.

[35] R. Jiang, D.N.P. Murthy, A study of Weibull shape parameter: properties and significance, Reliab. Eng. Syst. Saf. 96 (12) (2011) 1619–1626, https://doi.org/10.1016/J.RESS.2011.09.003.

[36] Website:NASA, POWER data methodology. [Online]. https://power.larc.nasa.gov/docs/methodology/ (accessed 20 May 2022).

[37] G. Falchetta, N. Stevanato, M. Moner-Girona, D. Mazzoni, E. Colombo, M. Hafner, The M-LED platform: advancing electricity demand assessment for communities living in energy poverty, Environ. Res. Lett. 16 (7) (2021), 074038, https://doi.org/10.1088/1748-9326/ac0cab.

[38] D.H. Fabini, D.P.L. de Baridó, A. Omu, J. Taneja, Mapping induced residential demand for electricity in Kenya, in: Proceedings of the Fifth ACM Symposium on Computing for Development, San Jose California USA, ACM, 2014, pp. 43–52, https://doi.org/10.1145/2674377.2674390.

[39] E. Soreng, Lithium Price Surge Could Charge Demand for Lead in Batteries, Reuters. [Online]. Disponibile su: https://www.reuters.com/markets/commodities/lithium-price-surge-could-charge-demand-lead-batteries-2021-12-16/.

[40] S. Pfenninger, et al., Opening the black box of energy modelling : strategies and lessons learned, Energy Strategy Rev. 19 (2018) 63–71, https://doi.org/10.1016/j.esr.2017.12.002.